

Biosynthesis of Carbon Spheres for Supercapacitor Electrode Application

Shicheng Wang*, Ling Ji and Xiaowen Tang

Beijing University of Technology, Beijing, 100124, P.R. China

*E-mail: shichengwangtech@foxmail.com

Received: 18 August 2017 / *Accepted:* 30 September 2017 / *Published:* 12 November 2017

In this work, corn starch was used for the synthesis of carbon spheres with a regular and perfect shape based on oxidation and carbonization. Carbon spheres typically exhibit large pore volume, high specific surface area, and a synergistic effect derived from mesopores and micropores. After preparation at 2600 °C, the as-prepared carbon spheres showed a low internal resistance (0.24 Ω) in KOH aqueous solution (6 M) and a specific capacitance of 311 F/g at a current density of 0.5 A/g. Even when the current density was as high as 10 A/g, the electrochemical capacitance was maintained at 196 F/g.

Keywords: Carbon spheres; Supercapacitor; Corn starch; Electrochemical performance; High temperature oxidation

1. INTRODUCTION

In recent years, energy use and greenhouse gas emissions have both increased with rising car ownership and vehicle utility. The International Energy Agency (IEA, 2009b) has predicted an average annual increase in global transport energy demand of 1.6% between 2007 and 2030. Consequently, energy consumption in automobiles has shifted significantly from petroleum to other substitutes [1, 2]. To meet the social and ecological requirements of green transportation, many automotive original equipment manufacturers have begun to focus on the development of more eco-friendly propulsion systems. Governments and automobile manufacturers have reached a consensus on new energy vehicles (NEVs) evolving from a “three horizontal and three vertical” development plan, where the “three vertical” corresponds to hybrid electric vehicle (HEV) [3-5], pure electric vehicle (PEV), and fuel cell vehicle (FCV), and the “three horizontal” indicates multi-energy vehicle systems for motor drive, control, and power management. As a primary technique for NEVs, electrical energy storage has

potential to be applied to future studies (and discoveries) based on the systems described above. The most common device used for electrical energy storage in vehicles is the supercapacitor, which is a type of electrochemical capacitor that can show high power density and prolonged cycle life; thus, such devices are desirable for applications in the eco-friendly energy field. In addition, supercapacitors can be used to bridge the energy and power gaps between traditional physical capacitors and secondary batteries/fuel cells [6-9]. Therefore, supercapacitors have been widely used in building advanced energy storage apparatus and electric vehicles.

Based on the mechanism for energy storage, supercapacitors can exist in two different forms, either as electrical double-layer capacitors (EDLCs) [10-13], which store energy on the electrode surface through fast charge adsorption/desorption, or pseudo-capacitors [14, 15], which store energy via surface Faradaic reactions between electrode materials and ions in the electrolyte. EDLC electrodes are typically composed of carbon materials [16, 17], including activated carbon [18, 19], carbon nanotubes, and graphene [20-23]. Ordered and uniform carbon materials with a porous structure and high specific surface area have been successfully used as the electrode in EDLCs [8-11]. Recently, the study of mesoporous carbon materials for supercapacitors has received intense interest, considering the suitability of the pore size and low microporous area fraction for EDLCs [23, 24]. Carbon spheres (CSs) are uniform, highly thermally stable, and exceptionally conductive with a high packing density, and have, therefore, been extensively used as adsorbents [25], catalyst supports [26, 27], and anodes in secondary lithium ion batteries [28]. However, there has been few studies of mesoporous carbon spheres (MCSs) for application in supercapacitors. The preparation of CSs has been proposed based on a wide range of carbon sources with a large number of synthetic approaches reported [29-31].

Starch is an eco-friendly, low cost, and renewable polymeric material that can be obtained in large quantities from a wide range of sources. In addition, starch is considered an ideal candidate for the replacement of synthetic polymer in efforts to eliminate environmental pollution. In this study, we synthesized carbon spheres using biosynthesized starch as the raw material. The physical properties of the biosynthesized starch-based carbon spheres were characterized using various experimental techniques. The starch-based carbon spheres were then used to fabricate the electrode material in a supercapacitor. The supercapacitor devices demonstrated improved performance due to the high surface area and excellent conductivity of the starch-based carbon electrode.

2. EXPERIMENTAL

Corn starch was purchased from a local supermarket. After oxidization in an oven at 210 °C for 24 h °C in air, the starch was carbonized in a tube furnace equipped with a programmable controller (used to vary the dwell time, final temperature, ramp rate, etc.). The reactor was exposed to a nitrogen flow immediately following carbonization. The final temperature of the furnace (600 °C) reached after ramping from ambient temperature (ramp rate: 2 °C/min) and was maintained for 60 min. The as-prepared corn starch was then given a final heat-treatment at 1000 °C, 1600 °C, 2000 °C, and 2600 °C (denoted as carbon spheres-1000, carbon spheres-1600, carbon spheres-2000, and carbon spheres-2600), respectively).

A D/Max 2500 X-ray diffractometer, with Cu K α radiation (40 kV, 200 mA, $\lambda = 1.54051 \text{ \AA}$), was used for structural characterization(). An ASAP-2010 surface area analyser was used to determine the adsorption/desorption of N₂ by Brunauer–Emmett–Teller (BET) analysis. Electrochemical impedance spectroscopy, galvanostatic charge/discharge (GCD) measurements, and cyclic voltammetry (CV) were carried out using a CHI 660D instrument equipped with a conventional three-electrode configuration. This setup consisted of a working electrode, a nickel foam counter electrode, and a Hg/HgO reference electrode. The working electrode was prepared by mixing a polytetrafluoroethylene binder, graphite, and carbon material (mass ratio: 8:1:1) with ethanol. After complete mixing, a paste was formed. This paste was then pressed into a 1 mm thick chip using a double roller machine. The chip was formed into a circular shape and pressed into nickel foam (pressure: 20 MPa) using a puncher. Finally, the electrode was dried and used as the working electrode. To ensure thorough diffusion of electrolyte into the sample pores, the working electrode was soaked in KOH solution (6 M) for 24 h. A multi-impedance test configuration was used for the electrochemical impedance spectroscopy, with an AC amplitude of 10 mV and frequency range of 10 kHz to 10 mHz.

3. RESULTS AND DISCUSSION

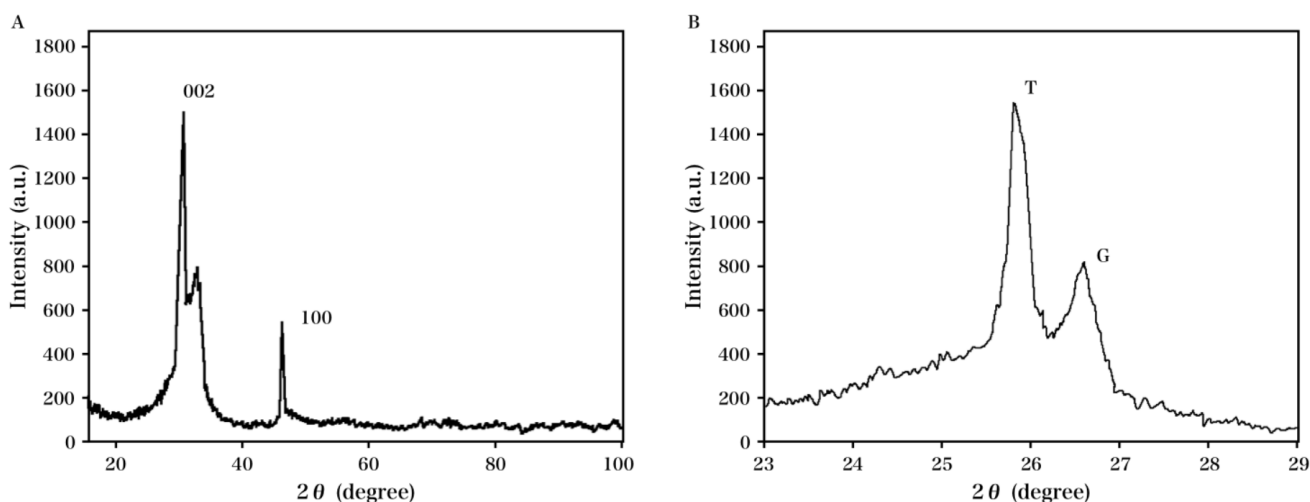


Figure 1. (A) XRD spectrum of the carbon sphere-2600. (B) Enlarged XRD spectrum of the 002 planes.

X-ray diffraction (XRD) is an effective tool for the micro-structural characterization of carbon materials. Fig. 1A shows the XRD profile of the carbon spheres obtained by graphitization at 2600 °C. The data show hard-carbon features for the graphitized material, as confirmed by both the asymmetry of the (100) peak and the broad bottom of the (002) peak. Fig. 1B shows the XRD pattern of the 002 planes, where A is an amorphous constituent characteristic of non-graphitizing carbon atoms. Upon increasing the temperature to 2600 °C, the A-constituent is partially transformed into the G-constituent, which suggests that the appearance of the G-constituent is indicative of graphitization. The

peak for the T-constituent is much narrower than that expected for typical turbostratic carbons, which indicates the formation of exceptionally thick crystallites. The interlayer distances for the carbon (002) planes in the T and G constituents were calculated to be 0.33758, and 0.34397 nm using the XRD data, respectively. Therefore, this phase creates a path for penetration throughout the bulk of the carbon sphere that is beneficial for application in supercapacitors where the entire electrode material can be used for energy storage [32, 33].

The carbon spheres were characterized by nitrogen adsorption and desorption isotherms (NADI) and pore size distribution (PSD) patterns, as shown in Fig. 2. The isotherms show sharp capillary condensation steps when the relative pressure is high, consistent with type IV curves. Hysteresis loops can be observed for the adsorption–desorption isotherms, which suggests that mesopores are present in the carbon spheres. The BJH model was used for calculation of the carbon sphere pore size distributions based on the adsorption branches of the isotherms [34]. As shown in Fig. 2B-D, the primary pore sizes in the carbon spheres were between 10 to 12 nm.

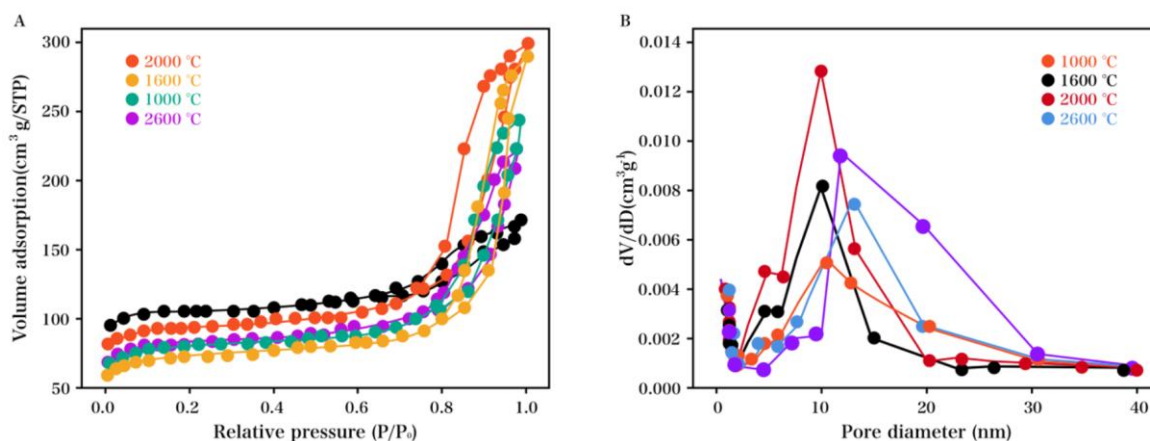


Figure 2. (A) Nitrogen adsorption and desorption isotherms of the carbon spheres. (B) Pore size distribution curves of the carbon spheres.

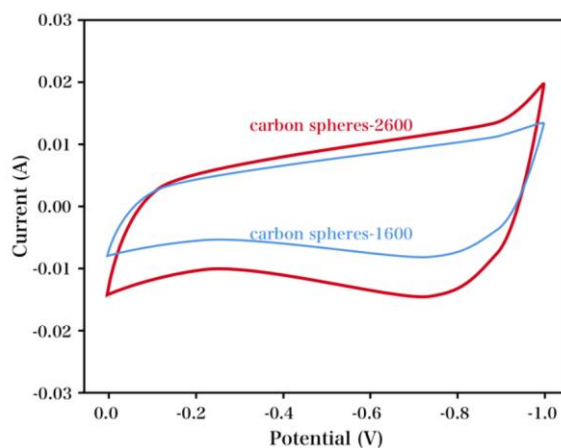


Figure 3. CV profiles of carbon spheres-1600 and carbon spheres-2600 in 6 M KOH aqueous solution obtained using a scan rate of 100 mV/s.

The carbon spheres-1600 electrode (CS-1600) and carbon spheres-2600 electrode (CS-2600) were characterized in KOH aqueous solution (6 M) by CV, as shown in Fig. 3 (scan rate: 100 mV/s). The specific capacitance of the carbon spheres as electrode material is proportional to the area contained within the CV curves [35]. As shown in Fig. 3A, carbon spheres-1600 show a quasi-rectangular shape for the CV loop, which suggests a dominant capacitive performance [36, 37]. The area of the quasi-rectangular CV loop for carbon spheres-2600 is larger than that for CS-1600 under a comparable potential window (Fig. 3). Therefore, carbon spheres-2600 show a more desirable capacitive performance compared with carbon spheres-1600 at a comparable sweep rate, due to the ample number of available micropores.

The CV profiles of carbon spheres-2600 in KOH aqueous solution (6 M) at varying scanning rates are shown in Fig. 4A. The data show that the CV profiles retain a quasi-rectangular shape for the voltammogram even at high scan rates of 100 and 500 mV/s, which suggests an exceptionally fast charge/discharge capacity of the carbon spheres-2600 used as a supercapacitor electrode [38]. By controlling the film thickness of carbon spheres-2600, we fully utilize the advantages of the ionic layer adsorption and reaction process to enable precise control of the charge storage capacity of the electrodes [39]. Other factors contributing to the remarkable electrochemical features observed include the short diffusion length for electrolyte ions (mesopores – micropores), ample sites for adsorption within each micropore, and fast ionic transfer within the mesopores [40]. In addition, the carbon spheres-600 exhibits a relatively wider quasi-rectangular CV area compared to other samples, which indicates carbon sphere-600 has higher specific capacitance due to the higher specific micropore surface and mesopore surface areas [41, 42].

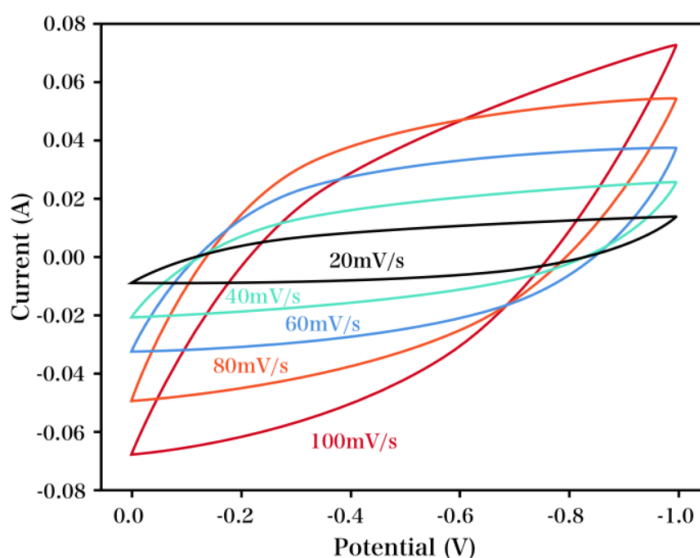


Figure 4. CV profiles of the carbon spheres-2600 electrode in 6 M KOH aqueous solution at varying scan rates.

Carbon spheres-2600 electrode in KOH aqueous solution (6 M) was also characterized by GCD patterns, as shown in Fig. 5 (loading current density: 0.5 A/g). The triangular shape in the GCD curves

and the linear time dependence of the potential for all samples confirms that the carbon spheres show capacitive performance characteristics of a supercapacitor. The specific capacitance for these carbon spheres was calculated at an applied current density of 0.5 A/g. The specific capacitance of carbon spheres-1600 is 170–266 F/g, and that of carbon spheres-2600 is 266 F/g; the latter is the highest among all the carbon spheres, which is ascribed to the high specific surface area. Activated carbon with high specific surface area generally shows a relatively good electrochemical capacitance. For example, Lu [43] reported the synthesis of activated carbon with a high specific micropore surface area of 3432 m²/g. Mesopores can facilitate the electron transfer process during fast charge/discharge operation, while micropores offer ample adsorption sites for electrolyte ion transfer. Thus, the synergistic effect of these two types of pore can contribute to an improved electrochemical capacitance.

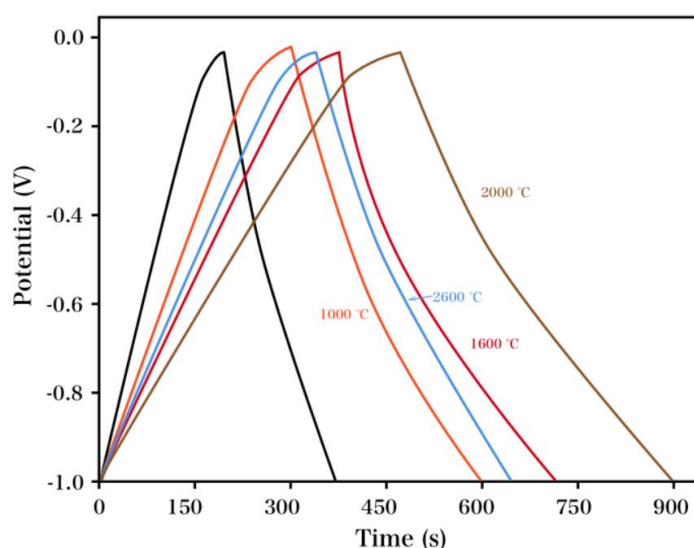


Figure 5. GCD patterns of carbon spheres electrodes in 6 M KOH aqueous solution under 0.5 A/g.

Figure 6 shows Nyquist plots of carbon spheres-1600 and carbon spheres-2600 in KOH aqueous solution (6 M) measured over a frequency range of 1 mHz to 10⁵ kHz. The data for carbon spheres-2600 show an almost vertical line as the slope becomes higher, indicating a Warburg resistance of charge saturation. Therefore, carbon spheres-2600 show high supercapacitor performance and desirable electrochemical behaviour. For both electrodes, the 45° line intercepts the intermediate frequency region, suggesting that ions are diffused into the electrode materials. Carbon spheres-1600 show an internal resistance of 0.57 Ω, but carbon spheres-2600 shows a much smaller internal resistance of 0.24 Ω, which indicates lower impedance at the electrolyte/carbon spheres-2600 interface. This can be assigned to efficient ion diffusion pathways in carbon spheres-2600 which shows large mesoporous domains.

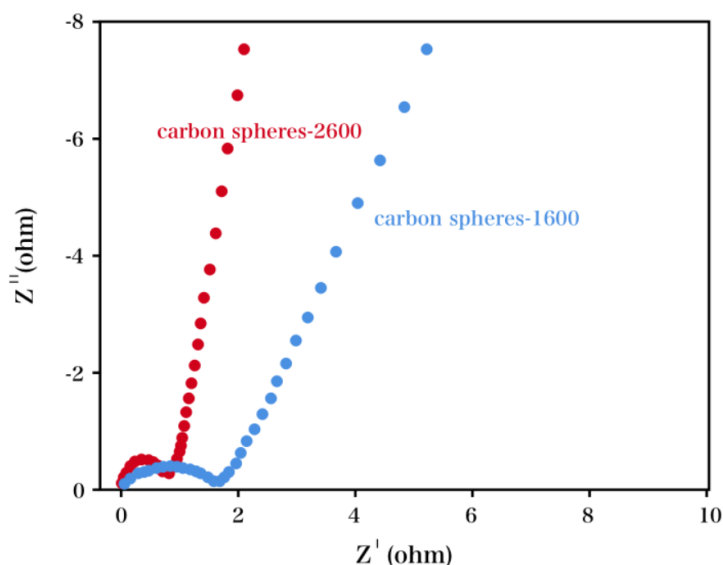


Figure 6. Nyquist plot of carbon spheres-1600 and carbon spheres-2600 electrodes in KOH solution (6 M) (1 mHz to 10^5 kHz).

The GCD patterns of carbon spheres-2600 in KOH aqueous solution (6 M) at varying applied current density are shown in Fig. 7. Even at a high current density of 15 A/g, the data show a triangle-shaped pattern, demonstrating the suitability of carbon spheres-2600 as the electrode for high loading current charge/discharge supercapacitors. The specific capacitance of carbon spheres-2600 at varying applied loading current density was also investigated. For a current density of 0.5 A/g, carbon spheres-2600 shows a specific capacitance of 311 F/g. The electrochemical capacitance showed only a nominal change from 196 to 157 F/g as the current density was increased from 10 to 15 A/g, respectively. These capacitances are superior to those obtained for similar, previously reported symmetrical systems. Table 1 shows a comparison of the maximum energy density of the carbon spheres with the energy density obtained for other materials as reported in the literature. The electrochemical capacitance of the activated carbon with high specific surface area is generally acceptable. Therefore, the synergistic effect produced by the combination of both ample micropores and large mesopores enables carbon spheres-2600 to show efficient charge/discharge properties with a large specific capacitance at high loading current density.

Table 1. Maximum energy density of the carbon spheres compared with materials from other reports.

Material	Maximum energy density (Wh/kg)	Reference
Prussian Blue modified positive electrode	7.68	[44]
Activated-N-doped graphene	66	[45]
GO/PPy	15	[46]
Papers coated with carbon nanotubes	41	[47]
Ni(OH) ₂ /MWCNT	17.9	[48]
CARBON SPHERES-2600	16.8	This work

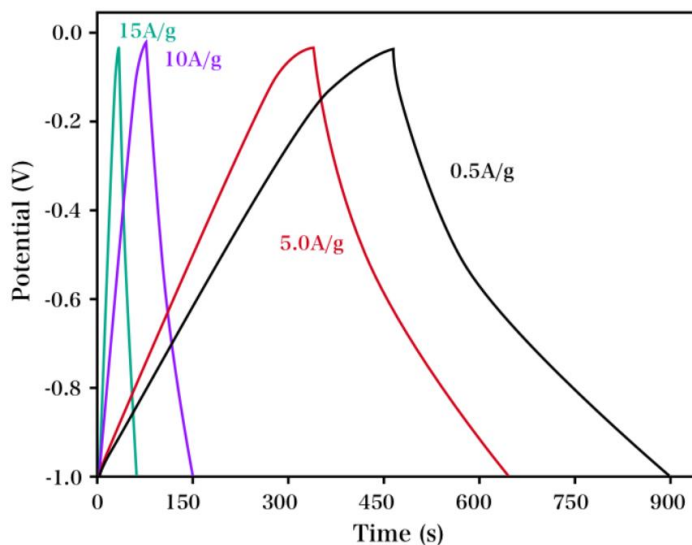


Figure 7. GCD patterns of carbon spheres-2600 used as the electrode material of a supercapacitor in 6 M KOH aqueous solution at current densities of 0.5, 5.0, 10, and 15 A/g.

4. CONCLUSIONS

In this work, a facile procedure based on the use of corn starch as a source material was implemented for the synthesis of carbon spheres. A high-temperature oxidization process was shown to significantly modify the biosynthetic starch and produce the final carbonized product. Supercapacitor devices built using carbon spheres-2600 as the electrode showed a low internal resistance (0.24Ω) in KOH aqueous solution (6 M) and a specific capacitance of 311 F/g at a current density of 0.5 A/g. Even when the current density was as high as 10 A/g, the electrochemical capacitance was maintained at 196 F/g.

ACKNOWLEDGEMENT

This work was supported by grants from “China's Post-doctoral Science Fund(2016M600888)” and “Beijing Postdoctoral Research Foundation”.

References

1. X. Yuan, X. Liu and J. Zuo, *Renewable and Sustainable Energy Reviews*, 42 (2015) 298.
2. J. Zhao, Z. Rao, Y. Huo, X. Liu and Y. Li, *Applied Thermal Engineering*, 85 (2015) 33.
3. K. Lo, *Renewable and Sustainable Energy Reviews*, 29 (2014) 508.
4. S. Wang, J. Fan, D. Zhao and Y. Wu, *Journal of Transport Economics and Policy (JTEP)*, 49 (2015) 98.
5. Z. Song, H. Hofmann, J. Li, J. Hou, X. Han and M. Ouyang, *Applied Energy*, 134 (2014) 321.
6. A.L. Lipson, B. Pan, S.H. Lapidus, C. Liao, J.T. Vaughey and B.J. Ingram, *Chemistry of Materials*, 27 (2015) 8442.
7. G. Ren, G. Ma and N. Cong, *Renewable and Sustainable Energy Reviews*, 41 (2015) 225.
8. F. Mwasilu, J.J. Justo, E.-K. Kim, T.D. Do and J.-W. Jung, *Renewable and Sustainable Energy Reviews*, 34 (2014) 501.

9. P. Zhang, F. Yan and C. Du, *Renewable and Sustainable Energy Reviews*, 48 (2015) 88.
10. Y. Guo, Z.-q. Shi, M.-m. Chen and C.-y. Wang, *Journal of Power Sources*, 252 (2014) 235.
11. Y. Zhao, M. Liu, L. Gan, X. Ma, D. Zhu, Z. Xu and L. Chen, *Energy & Fuels*, 28 (2014) 1561.
12. D. Kang, Q. Liu, J. Gu, Y. Su, W. Zhang and D. Zhang, *ACS nano*, 9 (2015) 11225.
13. L.-Q. Fan, J. Zhong, J.-H. Wu, J.-M. Lin and Y.-F. Huang, *Journal of Materials Chemistry A*, 2 (2014) 9011.
14. C. Zhang, L. Qian, K. Zhang, S. Yuan, J. Xiao and S. Wang, *Journal of Materials Chemistry A*, 3 (2015) 10519.
15. S.-M. Chen, R. Ramachandran, V. Mani and R. Saraswathi, *Int. J. Electrochem. Sci*, 9 (2014) 4072.
16. Q. Abbas, P. Ratajczak, P. Babuchowska, A. Le Comte, D. Bélanger, T. Brousse and F. Beguin, *Journal of the Electrochemical Society*, 162 (2015) A5148.
17. Q. Wang, J. Xu, X. Wang, B. Liu, X. Hou, G. Yu, P. Wang, D. Chen and G. Shen, *ChemElectroChem*, 1 (2014) 559.
18. S. Faraji and F.N. Ani, *Renewable and Sustainable Energy Reviews*, 42 (2015) 823.
19. M. Zhi, F. Yang, F. Meng, M. Li, A. Manivannan and N. Wu, *ACS Sustainable Chemistry & Engineering*, 2 (2014) 1592.
20. H. Sun, X. You, J. Deng, X. Chen, Z. Yang, J. Ren and H. Peng, *Advanced Materials*, 26 (2014) 2868.
21. D. Zhang, M. Miao, H. Niu and Z. Wei, *Acs Nano*, 8 (2014) 4571.
22. W. Gu and G. Yushin, *Wiley Interdisciplinary Reviews: Energy and Environment*, 3 (2014) 424.
23. Q. Zhou, Y. Li, L. Huang, C. Li and G. Shi, *Journal of Materials Chemistry A*, 2 (2014) 17489.
24. H.-J. Liu, W.-J. Cui, L.-H. Jin, C.-X. Wang and Y.-Y. Xia, *Journal of Materials Chemistry*, 19 (2009) 3661.
25. Y.Z. Jin, C. Gao, W.K. Hsu, Y. Zhu, A. Huczko, M. Bystrzejewski, M. Roe, C.Y. Lee, S. Acquah and H. Kroto, *Carbon*, 43 (2005) 1944.
26. Y. Wang, F. Su, J.Y. Lee and X. Zhao, *Chemistry of Materials*, 18 (2006) 1347.
27. J. Kim, J.E. Lee, J. Lee, J.H. Yu, B.C. Kim, K. An, Y. Hwang, C.-H. Shin, J.-G. Park and J. Kim, *Journal of the American Chemical Society*, 128 (2006) 688.
28. T. Spatzal, M. Aksoyoglu, L. Zhang, S.L. Andrade, E. Schleicher, S. Weber, D.C. Rees and O. Einsle, *Science*, 334 (2011) 940.
29. S. Ni, X. Wang, G. Zhou, F. Yang, J. Wang and D. He, *Journal of Alloys and Compounds*, 489 (2010) 252.
30. X. Guo, X. Liu, B. Xu and T. Dou, *Colloids and Surfaces A: Physicochemical and Engineering Aspects*, 345 (2009) 141.
31. G. Wu, Y. Cheng, Y. Ren, Y. Wang, Z. Wang and H. Wu, *Journal of Alloys and Compounds*, 652 (2015) 346.
32. R. Li, S. Wang, Z. Huang, F. Lu and T. He, *Journal of Power Sources*, 312 (2016) 156.
33. Y. Yang, D. Cheng, S. Chen, Y. Guan and J. Xiong, *Electrochimica Acta*, 193 (2016) 116.
34. D. Wu, X. Chen, S. Lu, Y. Liang, F. Xu and R. Fu, *Microporous and Mesoporous Materials*, 131 (2010) 261.
35. A.A. Khaleed, A. Bello, J.K. Dangbegnon, F.U. Ugbo, F. Barzegar, D.Y. Momodu, M.J. Madito, T.M. Masikhwa, O. Olaniyan and N. Manyala, *Journal of Materials Science*, 51 (2016) 6041.
36. M.F. El-Kady, V. Strong, S. Dubin and R.B. Kaner, *Science*, 335 (2012) 1326.
37. J. Qian, M. Liu, L. Gan, P.K. Tripathi, D. Zhu, Z. Xu, Z. Hao, L. Chen and D.S. Wright, *Chemical Communications*, 49 (2013) 3043.
38. G. Sun, J. Wang, K. Li, Y. Li and L. Xie, *Electrochimica Acta*, 59 (2012) 424.
39. Y. Xu, L. Wang, P. Cao, C. Cai, Y. Fu and X. Ma, *Journal of Power Sources*, 306 (2016) 742.
40. D. Tashima, E. Yamamoto, N. Kai, D. Fujikawa, G. Sakai, M. Otsubo and T. Kijima, *Carbon*, 49 (2011) 4848.
41. X. Cui, R. Lv, R.U.R. Sagar, C. Liu and Z. Zhang, *Electrochimica Acta*, 169 (2015) 342.

42. Z. Wang, W. Jia, M. Jiang, C. Chen and Y. Li, *Science China Materials*, 58 (2015) 944.
43. L. Wei, M. Sevilla, A.B. Fuertes, R. Mokaya and G. Yushin, *Advanced Functional Materials*, 22 (2012) 827.
44. P. Díaz, Z. González, R. Santamaría, M. Granda, R. Menéndez and C. Blanco, *Electrochimica Acta*, 212 (2016) 848.
45. Q. Fan, M. Yang, Q. Meng, B. Cao and Y. Yu, *Journal of The Electrochemical Society*, 163 (2016) A1736.
46. A. Singh and A. Chandra, *Journal of Applied Electrochemistry*, 43 (2013) 773.
47. Y.J. Kang, H. Chung, C.-H. Han and W. Kim, *Nanotechnology*, 23 (2012) 065401.
48. D.P. Dubal, G.S. Gungor, C.D. Lokhande and R. Holze, *Acs Applied Materials & Interfaces*, 5 (2013) 2446

© 2017 The Authors. Published by ESG (www.electrochemsci.org). This article is an open access article distributed under the terms and conditions of the Creative Commons Attribution license (<http://creativecommons.org/licenses/by/4.0/>).